

# Structure and Anticorrosion, Friction, and Wear Characteristics of Pure Diamond-Like Carbon (DLC), Cr-DLC, and Cr-H-DLC Films on AZ91D Mg Alloy

Xue-Jun Cui , Chuang-Ming Ning, Lun-Lin Shang, Guang-An Zhang, and Xiao-Qiang Liu

(Submitted May 4, 2018; in revised form November 30, 2018; published online January 11, 2019)

This study evaluated the protection against corrosion and wear afforded to AZ91D Mg alloy by coatings of hydrogen-free and low-Cr-doped hydrogenated diamond-like carbon (DLC) films. The microstructure and corrosion resistance were evaluated using scanning electron microscopy, atomic force microscopy, Raman spectroscopy, polarization curves, and neutral salt spraying tests. Wear tests were performed to investigate the friction and wear behaviors of the samples against 9Cr18 in humid air, deionized water, and 3.5 wt.% NaCl solution using a reciprocating sliding test in the ball-on-disk mode. The results showed that the more compact Cr-H-DLC film improved the corrosion resistance of the Mg alloy, whereas the Cr-DLC film accelerated the corrosion in the 3.5 wt.% NaCl solution. All Mg alloy samples coated with DLC films exhibited low coefficient of friction (COF) values and smaller wear volumes compared with those of bare substrate in air, water, or NaCl solution. The Cr-DLC film presented the lowest COF and wear rate in air, but the worst corrosion protection in air and NaCl solution, whereas the converse was found for the Cr-H-DLC film. Unfortunately, all coated samples showed limited protection ability because of pore defects in the films, high galvanic potential between the substrate and the buffer layer or film, and high electrical conductivity, which caused severe tribocorrosion of the Mg alloy during the wear tests in NaCl solution. The corrosion protection ability of DLC films is key to the wear resistance protection of Mg alloys in water or NaCl solution.

**Keywords** chromium, corrosion resistance, diamond-like carbon, friction and wear, hydrogen-free, magnesium alloys

## 1. Introduction

The characteristics of low-density, high strength-to-weight ratio, excellent machinability, and recyclability mean Mg alloys are one of the most promising lightweight metal groups for structural applications (Ref 1, 2). However, they have demonstrated poor resistance to both corrosion and wear in many environments that have restricted the range of their engineering applications (Ref 2, 3). It is considered that microstructural modification would not improve the performance of such alloys; therefore, an engineered surface coating would be required for their improved protection (Ref 2-6).

Diamond-like carbon (DLC) is a metastable form of amorphous carbon that contains a high fraction of  $sp^3$  bonds.

Recently, DLC coatings have been considered promising for improving the resistance of Mg alloys to corrosion and wear because of their high hardness, good adhesion, low coefficient of friction (COF), and chemical inertness (Ref 7-9). However, conventional DLC films adhere poorly to Mg alloys because of the large internal stresses associated with the  $sp^3$  bonds. Thus, the fundamental weakness of a DLC/Mg alloy system is the poor adhesion of the DLC film to the soft substrate because of mechanical incapability and high internal stresses. Metallic buffer layers such as Al (Ref 10), Ti (Ref 11), or Cr (Ref 12), prepared between a DLC film and a Mg alloy, have proven effective at improving adhesion; however, these buffer layers are limited to reducing the internal stresses of the DLC film. Some metals can be combined with carbon to form carbide, e.g., W (Ref 13), Ti (Ref 14), and Cr (Ref 15), or they can be dissolved into a DLC matrix, e.g., Al (Ref 16, 17). These have been found effective in both reducing the internal stresses and modifying the properties of DLC films on Mg alloys. Therefore, metal-doped DLC films have become a subject of considerable interest to the scientific community (Ref 10-25).

Cr is a carbide former that possesses an attractive combination of other properties such as resistance to corrosion and wear (Ref 26, 27), and considerable amounts of research have been performed in this area (Ref 15, 18-25). However, the emphasis of these earlier works has been on synthesis, structure and properties, while little attention has been paid to the protection of Mg alloys (Ref 15), especially their properties regarding friction and wear in water or corrosive media environments. Singh et al. (Ref 20) and Zou et al. (Ref 23) reported that low Cr ( $< 4.9$  at.%) doping could improve the excellent antiwear capacity of hydrogenated DLC films on Si (100) wafers, but no details of similar properties were reported

**Xue-Jun Cui**, School of Materials Science and Engineering, Sichuan University of Science and Engineering, Zigong 643000, China; and Key Laboratory of Marine Materials and Related Technologies, Ningbo Institute of Materials Technology and Engineering, Chinese Academy of Sciences, Ningbo 315000, China; **Chuang-Ming Ning** and **Xiao-Qiang Liu**, School of Materials Science and Engineering, Sichuan University of Science and Engineering, Zigong 643000, China; **Lun-Lin Shang** and **Guang-An Zhang**, State Key Laboratory of Solid Lubrication, Lanzhou Institute of Chemical Physics, Chinese Academy of Sciences, Lanzhou 730000, China. Contact e-mails: cxj\_2046@163.com and gazhang@licp.cas.cn.

for Mg alloys. Dai et al. (Ref 15) proved that hydrogenated DLC films with low Cr doping (2.34 at.%), which exhibited low internal stresses and high adhesion to a substrate, improved the wear resistance of Mg alloys under dry sliding conditions; however, no further investigations of their properties regarding friction and/or wear were performed in water or corrosive media conditions. DLC films can be divided into two groups based on their hydrogen content, i.e., hydrogenated and hydrogen-free carbon films (hereafter, H-DLC and pure DLC films, respectively). The influence of Cr-doped DLC (hereafter, Cr-DLC) film on the properties of friction and wear of Mg alloys has been neglected.

This study focused on low-Cr-doped H-DLC and pure DLC films deposited using an unbalanced magnetron sputter ion plating system. The purpose was to conduct systematic analysis of the protection capabilities of pure DLC, Cr-DLC, and Cr-H-DLC films for AZ91D Mg alloy in air, water, and corrosive media (i.e., 3.5 wt.% NaCl solution). The objectives were to develop better understanding of these DLC films and to explore an effective approach for enhancing the protection afforded to Mg alloys by DLC films.

## 2. Experimental

Commercial-grade AZ91D Mg alloy plates (30 × 25 × 2 mm) and thin Si (100) wafers were used as substrate materials. The chemical composition of the AZ91D Mg alloy is presented in Table 1. Prior to deposition of the DLC films, the Mg alloy plates were mechanically ground by up to #1200 SiC paper and then polished with diamond paste ( $\phi 2.5 \mu\text{m}$ ). Finally, all substrates were cleaned ultrasonically in absolute ethyl alcohol for 20 min and then dried in air.

Three types of DLC film, i.e., pure DLC, Cr-doped DLC (Cr-DLC) and Cr and H co-doped DLC (Cr-H-DLC) films, were deposited on the treated Mg alloy and Si wafer using pulsed DC equipment which is a patented closed-field unbalanced magnetron sputter ion plating system (UDP-650, Teer Coating Ltd.) at the State Key Laboratory of Solid Lubrication, Lanzhou Institute of Chemical Physics, Chinese Academy of Sciences. Cr (99.9%) and graphite targets with diameters of 60 mm were used. First, the treated substrates were placed in a vacuum chamber. After the base pressure was evacuated to a vacuum of  $5.0 \times 10^{-3}$  Pa, high-purity Ar gas (99.99%, 16 sccm) was introduced to sputter the substrates (bias voltage: – 500 V, frequency: 250 Hz, duty cycle: 80% and treatment time: 30 min) to remove surface contaminants. Next, to provide better adhesion, the Cr (target current: 3.5 A) transition layer was prepared (bias voltage: – 70 V, frequency: 250 Hz, duty cycle: 80%, and treatment time: 10 min) using high-purity Ar gas (30 sccm) under a pressure of 0.1 Pa. Finally, the pure DLC, Cr-DLC, and Cr-H-DLC films were fabricated on the Cr-coated substrates. The details of the deposition parameters are listed in Table 2.

**Table 1 Chemical composition of AZ91D Mg alloy (wt.%)**

| Composition   | Mg      | Al   | Si    | Cu     | Zn   | Mn   | Ni      | Fe     |
|---------------|---------|------|-------|--------|------|------|---------|--------|
| Mass fraction | Balance | 8.91 | 0.016 | 0.0025 | 0.84 | 0.32 | 0.00045 | 0.0022 |

A field emission scanning electron microscope (FE-SEM, HITACHI SU8020, Japan) was used to investigate the surface and cross-sectional morphologies of the DLC films. Atomic force microscopy (AFM, Benyuan CSPM4000, China) was used to characterize the surface topography and roughness of the films. A digital camera and optical microscopy were also used to observe the surface morphologies of the coated and worn samples, respectively. Raman spectroscopy (Horiba Jobin–Yvon LabRAM HR800, France) with an Ar<sup>+</sup> beam at the wavelength of 532 nm was used to measure the atomic bonds of the films on the Si substrate.

The internal stress of the DLC coatings was evaluated using a coating stress tester (FST-1000). At least four measurements were taken for different locations in the coatings, and the average value was regarded as the internal stress of the coating. The adhesion strength of the DLC coatings was measured using a multifunctional material surface performance tester (MFT-4000). The coated samples were fixed horizontally on the loading platform; the loading speed was 10 N/min, the critical load was 0 N, the termination load was 10 N, and the scratch length was 5 mm. The loading force and friction force ranged as – 0.02 to 0.01 N and – 0.02 to 0 N, respectively. The scratch was observed by optical microscopy.

Polarization curves of the bare and DLC-coated Mg alloy were determined using an electrochemical work station (Autolab, PGSTAT 302 N) in 3.5 wt.% NaCl solution. A conventional three-electrode cell was used, i.e., a saturated calomel electrode was used as the reference electrode, a Pt sheet (4 cm<sup>2</sup>) was used as the counter electrode, and the exposed area (0.5 cm<sup>2</sup>) of the sample was used as the working electrode. To ensure the samples were stabilized in the NaCl solution, open-circuit potential (OCP) tests were carried out. Polarization tests could not be conducted until the OCP changes were  $\pm < 5$  mV during the 5-min period of measuring the potentials. The scan rate was 1 mV/s and the scanning region was set from – 0.80 to + 1.5 V with respect to the OCP. Each sample was tested at least three times to ensure reliability and reproducibility. The corrosion parameters were calculated using electrochemical software (CHI, version 12.23, USA). Based on the mostly linear polarization behavior in the Tafel region ( $\pm 100$  mV with respect to the corrosion potential), the polarization resistance ( $R_p$ ) values are determined using Eq 1, which is the Stern–Geary equation.

$$R_p = \frac{b_a b_c}{2.303 i_{\text{corr}} (b_c - b_a)} \quad (\text{Eq 1})$$

To determine the corrosion resistance of the bare and coated Mg alloy, a neutral salt spray (NSS) test was performed according to GB T 10125-2012/ISO 9227:2002. Three different samples of each type of DLC were prepared and tested for 8 h. Following the NSS test, the corrosion product was cleaned using soapy water.

Friction experiments were performed using a ball-on-disk tribometer (CSM) at room temperature ( $22 \pm 2$  °C) with

**Table 2 Deposition parameters of three kinds of DLC films**

| Films   | Cr      | DLC     | Cr-DLC  | Cr-H-DLC |
|---|---------|---------|---------|----------|
| Vacuum, Pa  | 0.1     | 0.1     | 0.1     | 0.1      |
| Ar flowing rate, sccm                             | 16      | 16      | 16      | 30       |
| C <sub>4</sub> H <sub>10</sub> flowing rate, sccm | 0       | 0       | 0       | 30       |
| Distance of target to substrate, mm               | 150     | 150     | 150     | 150      |
| Current of Cr target, A                           | 3.0     | 0       | 0.38    | 0.38     |
| Current of graphite target, A                     | 0       | 3.5     | 3.5     | 3.5      |
| Negative bias voltage, V                          | 70      | 150     | 150     | 150      |
| Deposition temperature, °C                        | 150-200 | 150-200 | 150-200 | 150-200  |
| Deposition time, min                              | 30      | 300     | 300     | 300      |

relative humidity of  $27 \pm 2\%$  in air, deionized (DI) water and 3.5 wt.% NaCl solution. During the reciprocating friction tests, a 9Cr18 steel ball (diameter: 6 mm) was used as the friction counter body, the reciprocating length was 5 mm, sliding time was 2000s and sliding frequency was 5 Hz. The total sliding distance was 100 m. The normal load was 5 N in air and 1 N in both DI water and 3.5 wt.% NaCl solution. The COF values were obtained directly from the tribometer computer. After the friction tests, the worn surfaces were observed as described above, and their wear volumes were measured using a 2-D noncontact optical profilometer (KLA-Tencor D-100, USA). The specific wear rate ( $W$ ) of the coated samples is calculated according to Eq 2.

$$W = V / (F \times L) \quad (\text{Eq 2})$$

where  $V$  is the wear volume of the wear track,  $F$  is the normal load, and  $L$  is the sliding distance.

### 3. Results and Discussion

#### 3.1 Surface Characterization

Figure 1 shows the examples of the surface morphologies of the DLC-coated samples. The pure DLC and Cr-DLC films on the Mg alloy appear light gray, and the Cr-H-DLC film appears black. The DLC films present typical smooth, imporous, and crack-free surface macroscopic morphologies (Fig. 1a1, b1, and c1), indicating good adhesion between the DLC films and the Mg alloy. However, some limitations are observable when magnified using SEM. The pure DLC and Cr-DLC films show microcracking among the cluster particles (Fig. 1a2 and a3, b2, and b3), whereas the Cr-H-DLC film still shows a dense structure (Fig. 1c2 and c3). Thus, it can be considered that the microcracking could provide channels for corrosive media in an aggressive environment that would weaken corrosion resistance (Ref 28). The Mg alloy coated with Cr-H-DLC shows good corrosion resistance. Additionally, the typical AFM images of the DLC films prove they have smooth surfaces because of the low roughness (Fig. 1a4, b4, and c4). In comparison, the Cr-DLC film shows relatively high roughness, implying good adhesion to the substrate and a low rate of wear in air (Ref 29).

Figure 2 shows cross-sectional SEM images of DLC films deposited on Si wafers. In each image, the cross sections exhibit evident differences. A columnar microstructure can be observed in the cross section of the pure DLC film (Fig. 2a), whereas the structure is indistinct in the cross sections of the Cr-DLC and Cr-H-DLC films. The DLC (top) and Cr (bottom)

can be distinguished in the cross sections of the pure DLC and Cr-H-DLC films (Fig. 2a and c), whereas they are difficult to observe in the cross section of the Cr-DLC film. Moreover, a microcrack is visible between the DLC film and the Cr interlayer (Fig. 2a). Thus, it can be concluded that a Cr-doped DLC film is matched more easily than a pure DLC film with a Cr buffer interlayer, which implies that a Cr-DLC film would have a high growth rate (Ref 12, 15, 23). Table 4 shows that the film thickness increases from 3.60  $\mu\text{m}$  for the pure DLC film to 3.78  $\mu\text{m}$  for the Cr-DLC film. Additionally, it can be observed that the Cr-H-DLC film shows a more compact cross-sectional structure. This is in agreement with the thickness of the Cr-H-DLC film, which is lower than that of the pure DLC film (Table 4), indicating that hydrogen doping would improve the compactness of a DLC film (Ref 30).

Generally, the Raman spectra of a DLC film can be fitted using two Gaussians peaks: the G peak and the D-peak. The G-band at around 1540-1580  $\text{cm}^{-1}$  represents graphite, and the D-band at around 1350  $\text{cm}^{-1}$  represents a disordered graphite-like structure (not diamond) (Ref 31). According to an earlier investigation (Ref 32), the structure of a DLC film depends strongly on energy. Thus, the DLC films of this study show the typical shape of a DLC spectrum, as shown in Fig. 3. Usually, the G-band is derived from the  $E_{2g}$  symmetric vibrational mode of the graphite layers of  $\text{sp}^2$  microdomains, whereas the D-band is assigned to bond-angle disorder in the graphite structure, induced by linking with  $\text{sp}^3$  carbon atoms and the lack of long-distance order in graphite-like microdomains (Ref 31, 33, 34). Thus, the G-band for the Cr-DLC film is shifted toward higher frequencies, reflecting the increase in graphite-like microdomains in the Cr-DLC film, which is in agreement with the reference (Ref 15). In contrast, the increase in diamond-like microdomains in the Cr-H-DLC film is reflected in the shift of its G-band toward lower frequencies. Moreover, the decreasing intensity of the D-peak in the Cr-H-DLC film demonstrates the disordering of the amorphous carbon film (Ref 35). Additionally, the  $I_D/I_G$  ratio increases from 2.2 for the pure DLC film to 3.6 for the Cr-DLC film, whereas it decreases to 1.1 for Cr-H-DLC film. This suggests the Cr-DLC film has an  $\text{sp}^2$ -rich microstructure, whereas the Cr-H-DLC film has an  $\text{sp}^3$ -rich microstructure. Therefore, in comparison with a pure DLC film under normal dry friction conditions, it can be concluded that the Cr-DLC and Cr-H-DLC films would show lower and higher COF values, respectively.

#### 3.2 Internal Stress and Adhesion

The internal stress of the DLC films is also shown in Table 4. The internal stress of the pure DLC, Cr-DLC, and Cr-



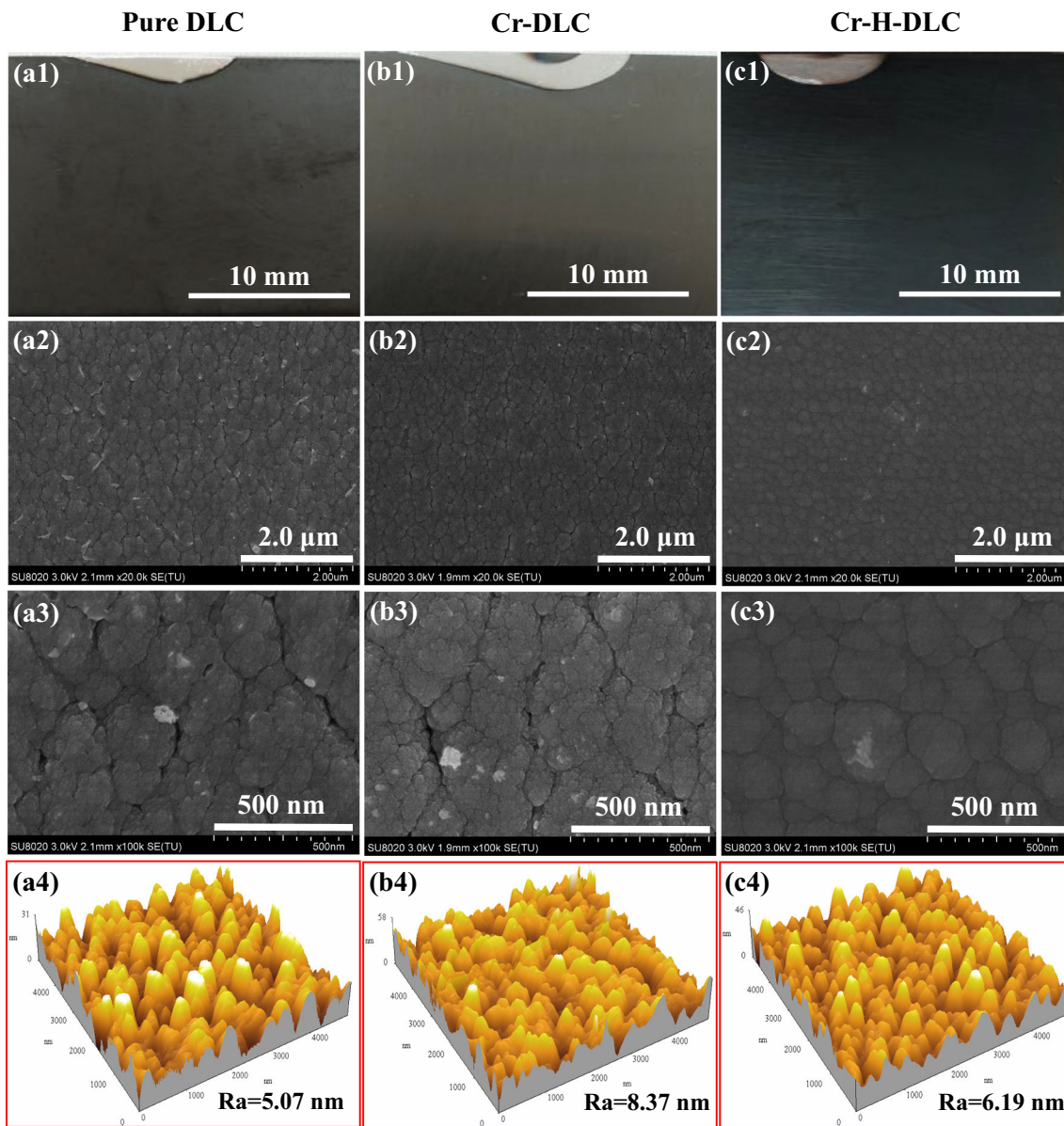


**Fig. 1** Optical photographs (a1-c1), SEM images (a2-c2, a3-c3), and AFM images (a4-c4) of the coated Mg alloys: (a1-a4) pure DLC; (b1-b4) Cr-DLC; (c1-c4) Cr-H-DLC. Note: a1, b1, and c1 are the DLC-coated Mg alloys; (a2-a4), (b2-b4), and (c2-c4) are the DLC-coated Si wafers

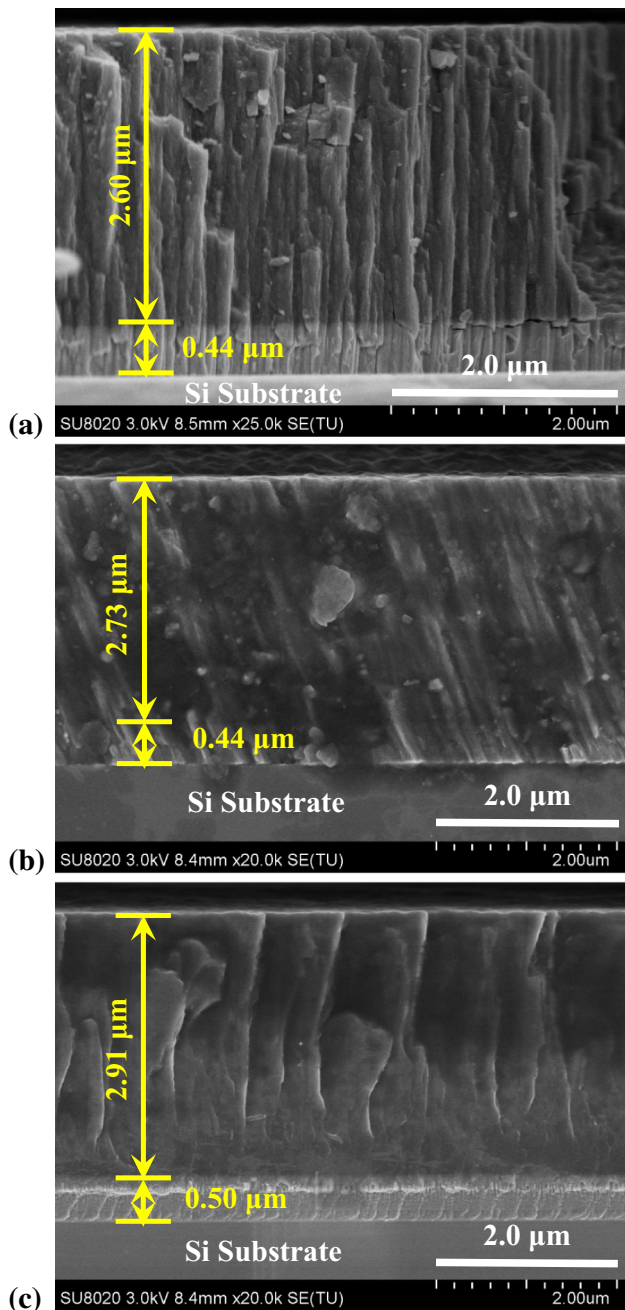
H-DLC films is 1.18, 1.26, and 2.71 GPa, respectively. Some CrC phases can be formed in the amorphous carbon matrix. The Cr-C bond is longer than the C-C bond, thereby increasing the internal stress (Ref 13). Additionally, the increase in the internal stress in the Cr-H-DLC films should be contributed to increasing the  $sp^3$  fraction, as indicated by the  $I_D/I_G$  ratio in Fig. 3.

Typically, the lower the internal stress of the DLC films, the higher the adhesion strength. However, the Cr-DLC, and Cr-H-DLC films showed higher adhesion strength than the pure DLC film in Fig. 4 despite possessing a relatively high internal stress. This can be ascribed to the enhanced interface bonding between the DLC films and Cr layer due to Cr doping (Ref 15). Meanwhile, the adhesion strength of the Cr-H-DLC film (7.4 N) was lower than that of the Cr-DLC film (8.1 N) due to its highest internal stress. Therefore, good interface adhesion not only depends on the low internal stress, but also on strong interface bonding.

### 3.3 Corrosion Resistance

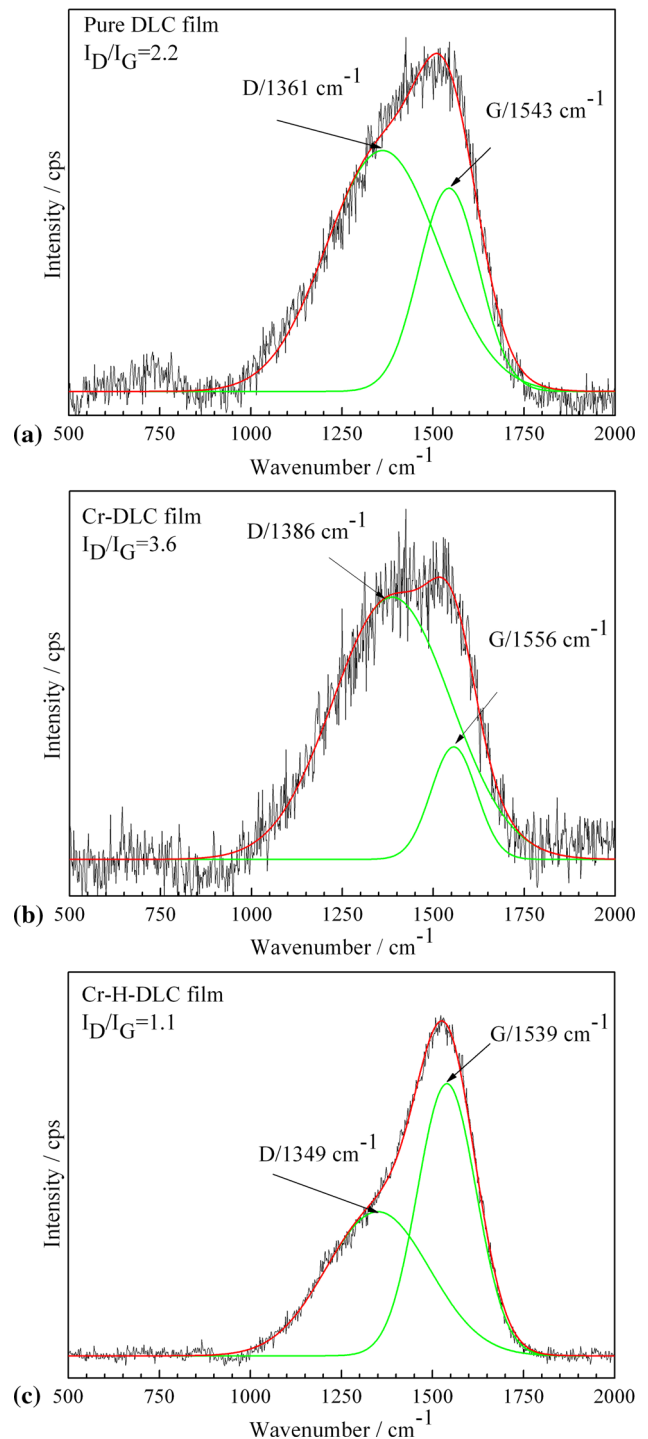
Figure 5 exhibits the polarization curves of the bare and coated Mg alloy in the 3.5 wt.% NaCl solution. The fitting results are listed in Table 3. Compared with the bare Mg alloy, the current density values of the DLC- and the Cr-H-DLC-coated samples decrease and the corrosion potential values shift slightly toward the positive direction; however, the Cr-DLC-coated sample shows the converse. It can be concluded that both the DLC and Cr-H-DLC films improve the corrosion resistance of the Mg alloy, whereas the Cr-DLC film fails to offer protection. According to Faraday's law, lower corrosion current density means higher corrosion resistance. Therefore, of all the samples tested, the Cr-H-DLC film provides the best corrosion protection for the Mg alloy.

Figure 6 shows the appearance of both bare and coated Mg alloy samples after the NSS tests. During the NSS tests, the surfaces of the bare and of the DLC- and Cr-DLC-coated



**Fig. 2** Cross-sectional SEM images of (a) pure DLC, (b) Cr-DLC, and (c) Cr-H-DLC films on Si wafers

samples revealed the adhesion of considerable numbers of NaCl particles after 4 h (Fig. 6a1, b1, and c1), whereas the Cr-H-DLC-coated sample showed much less adhesion by NaCl particles (Fig. 6d1). In fact, it was observed that the bare Mg alloy lost its metallic luster once the NSS test began, indicating that corrosion had occurred. The DLC- and Cr-DLC-coated samples developed some white pits or corrosion products after 2 h, but the Cr-H-DLC-coated sample did not. During the NSS test, the Cr-H-DLC-coated sample showed no evidence of corrosion for 6 h. Considerable numbers of white salt particles covered the dried surfaces of the bare and coated samples after 8 h of the NSS tests (Fig. 6a2-d2), resulting in the invisible corrosion appearance. However, the effects of corrosion were visible after the samples had been rinsed with soapy water and



**Fig. 3** Raman spectra of the DLC films on Si wafer

DI water. Catastrophic corrosive topography was found on the surface of the bare Mg alloy. There was no coating, but some corrosion pits were observed on the Cr-DLC-coated sample. Although corrosion pits were not obvious on the DLC- and Cr-H-DLC-coated samples, some white regions were visible, which represented the residues of corrosion pits that formed during the tests (Ref 10). Comparatively, among the samples tested, the Cr-H-DLC film retarded the corrosion of the Mg alloy (Fig. 6), verifying the conclusion derived following the polarization test.



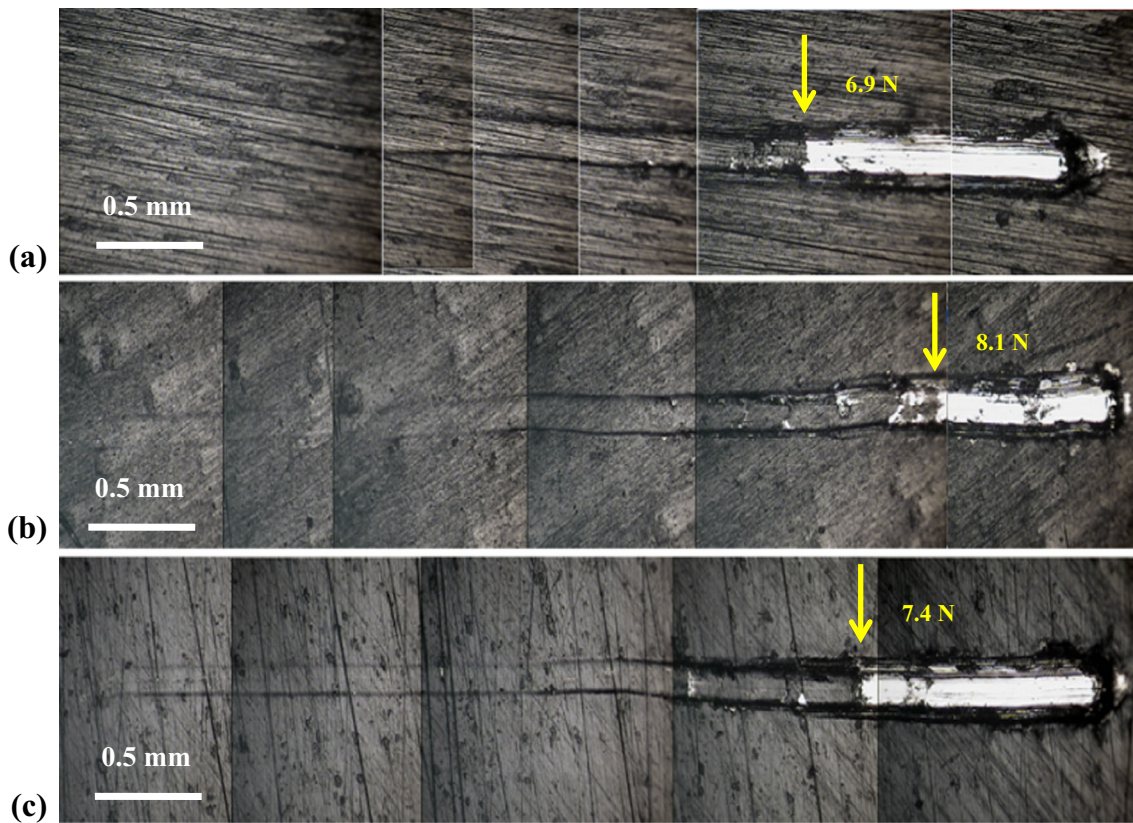


**Fig. 4** Scratch appearance of the coated AZ91D Mg alloys: (a) DLC; (b) Cr-DLC; (c) Cr-H-DLC

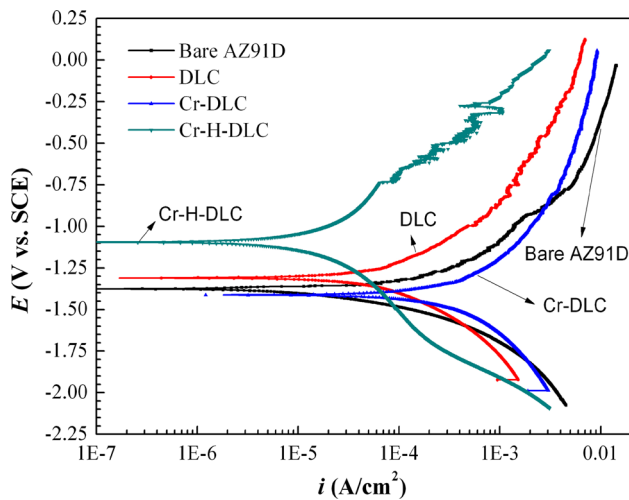


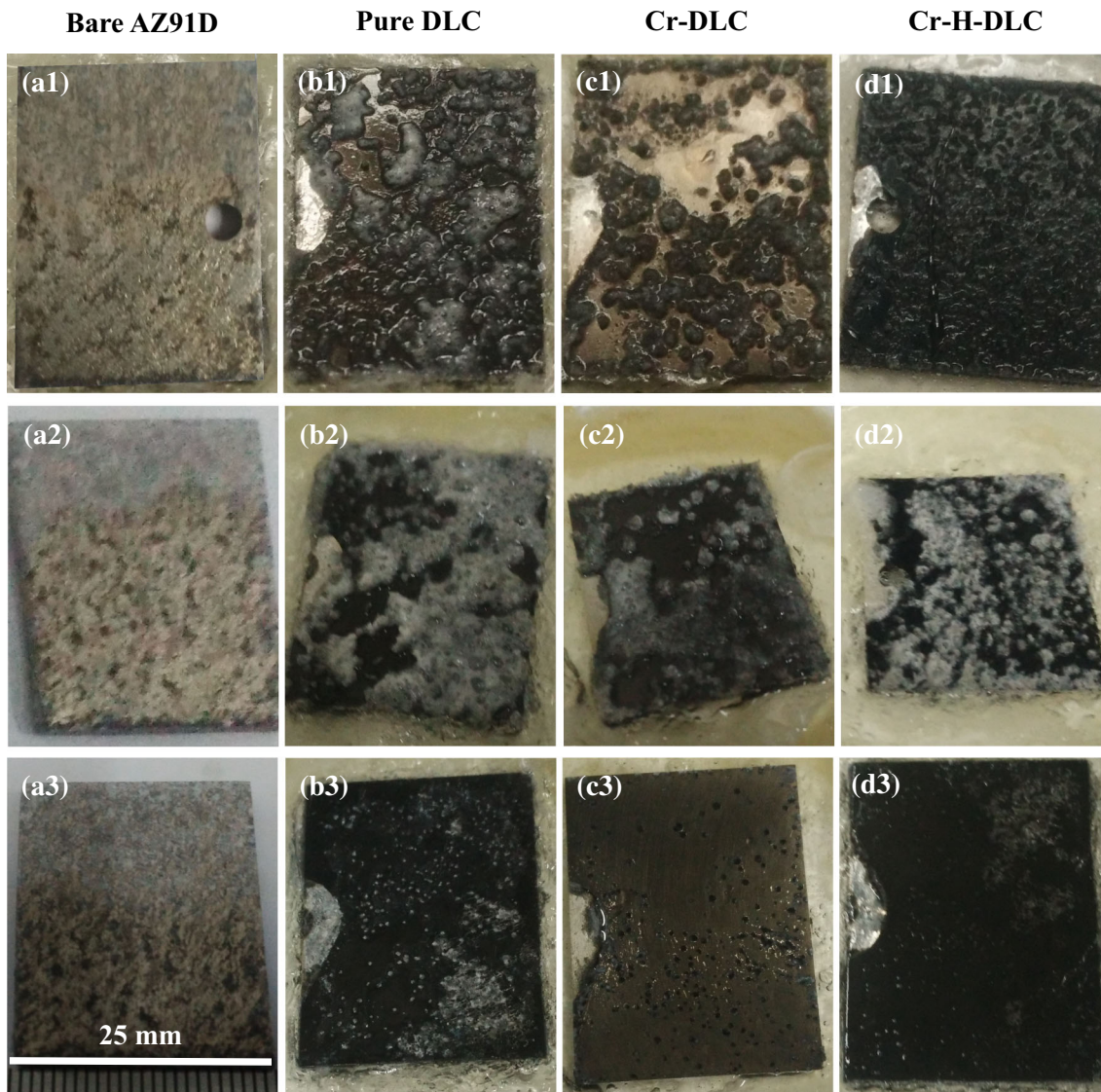
**Fig. 5** Polarization curves of the bare and DLC-coated AZ91D Mg alloys

Pinholes are inevitable defects found in PVD or CVD coatings (Ref 36-38). Moreover, pores with diameters of approximately 0.5 nm are always distributed randomly within such films, even in high-quality DLC films (Ref 39, 40), as illustrated in the films prepared for this study (Fig. 1 and 2). Water molecules have diameters of approximately 0.32 nm; therefore, they are able to permeate DLC films easily through these pores. It can be speculated that water molecules with corrosive ions such as  $\text{Cl}^-$  could permeate films easily when placed within a Cl-containing environment. Once corrosive

**Table 3** Fitting results of the polarization curves from Fig. 5

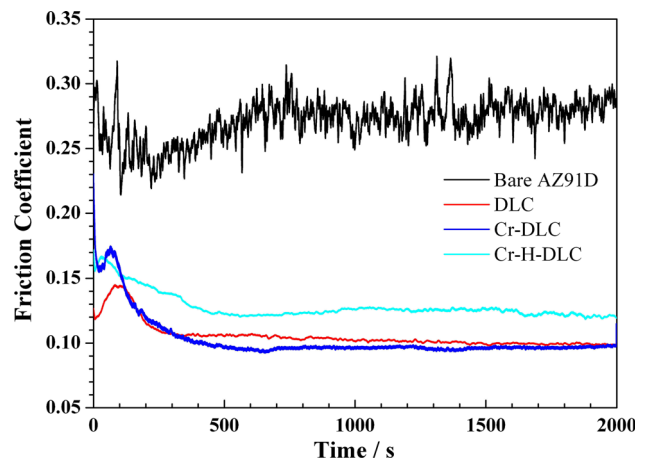
|   | Bare AZ91D | DLC  | Cr-DLC | Cr-H-DLC |
|---|------------|------|--------|----------|
| $-E_{\text{corr}}$ , mV vs. SCE           | 1399       | 1311 | 1422   | 1092     |
| $i_{\text{corr}}$ , $\mu\text{A cm}^{-2}$ | 142.9      | 44.3 | 344.6  | 14.5     |
| $b_a$ , mV/dec                            | 148        | 242  | 156    | 226      |
| $-b_c$ , mV/dec                           | 122        | 195  | 183    | 190      |
| $R_p$ , $\text{k}\Omega$                  | 2.11       | 9.84 | 1.33   | 35.72    |

media penetrate via these pores to the interface between the film and the substrate, galvanic cells would be produced between the electrochemically nobler DLC/Cr layer and the active Mg substrate (Ref 10, 28). Then, the Mg substrate, as the anode, would begin to dissolve, and the DLC/Cr layer, as the cathode, would become involved in hydrogen evolution in these pores. The reaction would lead to the accumulation of certain corrosion products in the pores; however, these products would not prevent further reaction because of the porous nature of  $\text{Mg}(\text{OH})_2$ , which is the principal component of the corrosion products (Ref 41). Subsequently,  $\text{Cl}^-$  would tend to transform the  $\text{Mg}(\text{OH})_2$  into soluble  $\text{MgCl}_2$  (Ref 42, 43). This would lead to enlargement of corrosion pits, resulting in visible corrosive pits on the surface of the Mg alloy coated with the pure DLC film (Fig. 6b3). However, galvanic corrosion could be hindered by the insulating effect of a DLC film (Ref 10) such that DLC-coated Mg alloy would show better anticorrosion properties than bare substrate. Singh et al. (Ref 20) reported that DLC films with 4.8 at.% Cr contain crystalline chromium carbide nanoclusters embedded within an amorphous DLC matrix. Dai



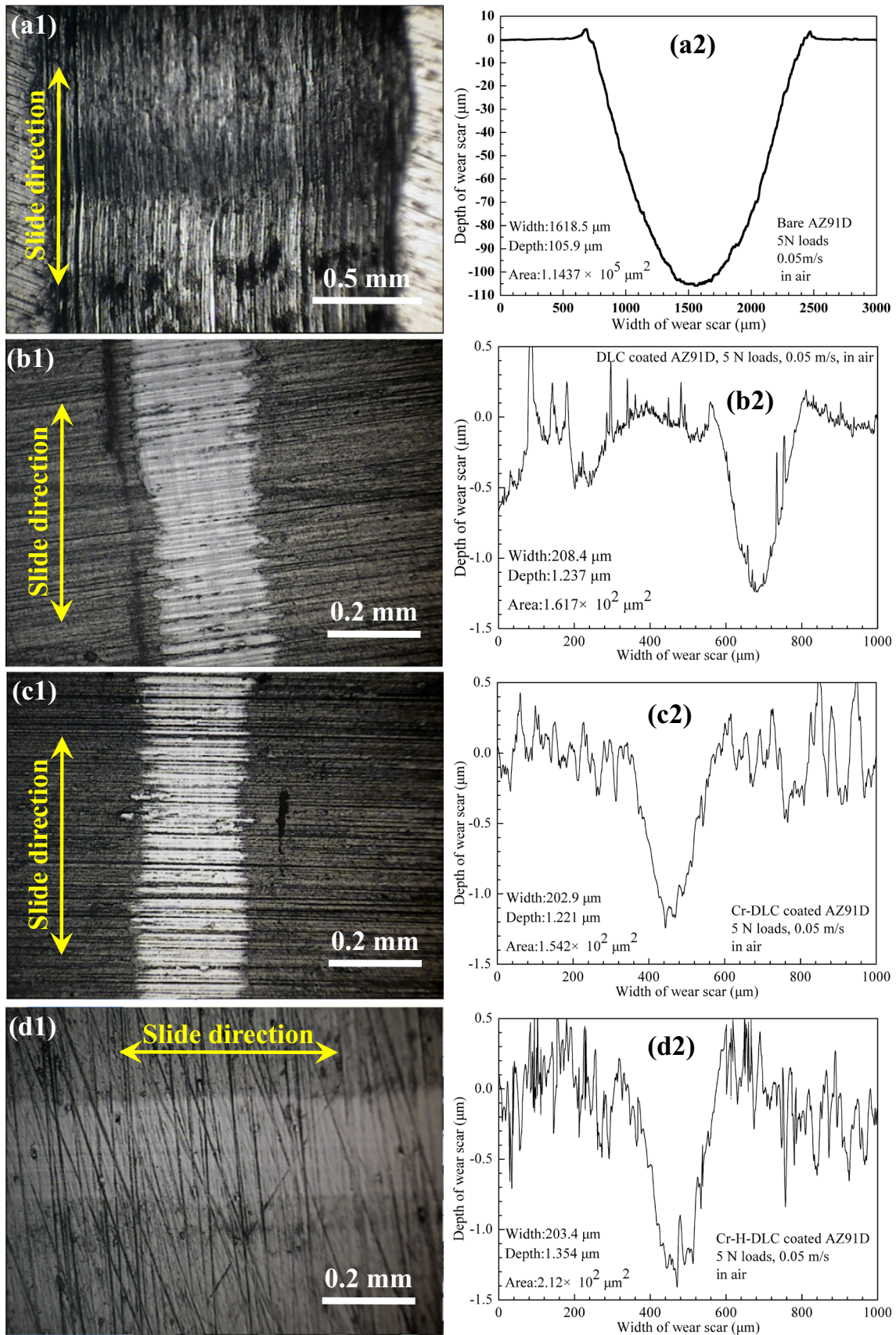
**Fig. 6** Appearance of the bare and DLC-coated AZ91D Mg alloys after NSS test. (a1-d1): 4 h with corrosion products; (a2-d2): 8 h with corrosion products; (a3-d3): 8 h without corrosion products

et al. (Ref 44) stated that Cr-DLC film with low Cr content ( $< 8.42$  at.%) doping is an amorphous DLC structure with dispersed metallic-like Cr. Therefore, Cr doping should increase the electrical conductivity of a DLC film. It can be speculated that some corrosion microcells with large cathodes and small anodes would be formed in the micropores within a Cr-DLC film, which would accelerate both the corrosion of the Mg alloy and the deterioration of the Cr-DLC film. Thus, compared with the DLC-coated sample, the Cr-DLC-coated sample in this study exhibited less corrosion resistance (Fig. 5) because of synergistic effects between poor compactness (Fig. 1b3), the large cathode and small anode, and good electrical conductivity. Wu (Ref 12) and Dai et al. (Ref 15) proved that Cr as an interlayer did not enhance the corrosion resistance of DLC/Mg alloy systems in Cl-containing solutions. This was attributed to the formation of galvanic cells between the substrate and the Cr layer in the region of through-thickness defects. Zeng (Ref 28) and Panjan et al. (Ref 36) suggested that



**Fig. 7** COFs of the bare and DLC-coated AZ91D Mg alloys as a function of the sliding time at 5 N load in air with  $27 \pm 2\%$  RH



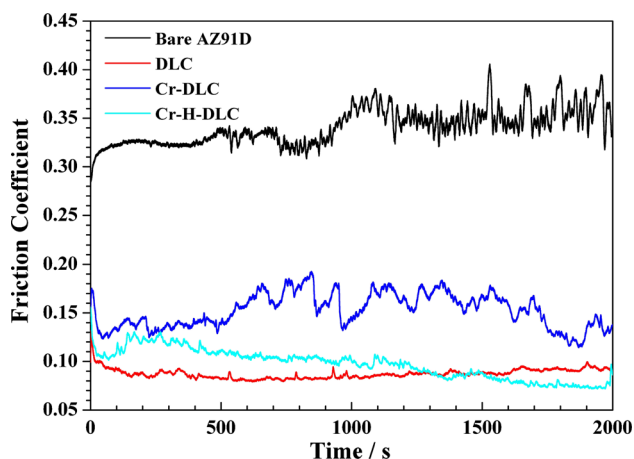


**Fig. 8** Microscope images and sectional morphologies of the wear scar of the bare and coated AZ91D Mg alloys at 5 N load in air with  $27 \pm 2\%$  RH. (a1, a2) bare AZ91D; (b1, b2) DLC; (c1, c2) Cr-DLC; (d1, d2) Cr-H-DLC



**Table 4 Parameters of the DLC films**

| Specimen   | Thickness, $\mu\text{m}$ | Internal stress, GPa | Wear rate/ $\times 10^{-6} \text{ mm (N m)}^{-1}$ |       |               |
|------------|--------------------------|----------------------|---|-------|---------------|
|            |                          |                      | Air   | Water | NaCl solution |
| Bare AZ91D | ...                      | ...                  | 1143.7  | 146.4 | 264.5         |
| Pure DLC   | 3.60                     | - 1.18               | 1.617   | 2.453 | 4.420         |
| Cr-DLC     | 3.78                     | -1.26                | 1.542   | 4.321 | 5.709         |
| Cr-H-DLC   | 3.50                     | - 2.71               | 2.120   | 1.314 | 3.054         |

**Fig. 9** COFs of the bare and coated AZ91D Mg alloys as a function of the sliding time at 1 N load in DI water

the corrosion resistance of DLC films was compromised by pores within the films. Therefore, among the three coated samples of this study, the Cr-H-DLC-coated sample showed the best corrosion resistance because of the compactness of the Cr-H-DLC film (Fig. 1c3), which might reduce the numbers of pores (i.e., corrosion microcells).

### 3.4 Friction and Wear

**3.4.1 In Humid Air.** Figure 7 shows COF values of bare and DLC-coated Mg alloy samples as a function of sliding time under loads of 5 N in air with relative humidity of  $27 \pm 2\%$ . It can be seen that the COF of the bare Mg alloy changes considerably, while that of the coated samples remains stable. The stable COF values for the bare and the pure DLC-, Cr-DLC-, and Cr-H-DLC-coated Mg alloy samples vary in the ranges of 0.25-0.30, 0.10-0.11, 0.09-0.10, and 0.12-0.13, respectively. The coated samples show better friction behavior in humid air in comparison with the bare substrate. The frictional curve of the Cr-H-DLC-coated sample exhibits a long running-in distance and a higher COF value than both the pure DLC- and the Cr-DLC-coated samples, indicating that the Cr-H-DLC-coated sample has a higher wear rate than the pure DLC and Cr-DLC samples. The COF of the Cr-DLC sample is lower than that of the pure DLC film in the stable step, which is in agreement with the results of the Raman spectroscopy.

Figure 8 shows the microscopy images and sectional profiles of the wear scars of bare and coated Mg alloy samples under loads of 5 N in air with relative humidity of  $27 \pm 2\%$ . The bare Mg alloy presents deeper and wider wear tracks compared with the coated samples; it also has the highest wear rate in Table 4. It is evident that the DLC films show better wear behavior (Fig. 8b1,

c1, and d1), although they have different wear rates, i.e., in order from large to small: Cr-H-DLC > pure DLC > Cr-DLC. This shows that the Cr-DLC-coated Mg alloy has good friction and wear behaviors in humid air.

The friction and wear behaviors of DLC films are correlated primarily with composition, microstructure and sliding environment (Ref 9, 23, 29, 45, 46). The  $I_D/I_G$  ratio of the pure DLC film is about 2.2, whereas that of the Cr-DLC film increases to 3.6 after the low Cr content was doped into the pure DLC film (Fig. 3). This implies that Cr doping induced a transformation of  $sp^3$  to  $sp^2$ , meaning the Cr-DLC film became more graphite-like (Ref 13). Moreover, the DLC film with low Cr content is characterized by amorphous DLC with Cr atoms dispersed within it (Ref 44). Thus, the Cr-DLC film exhibits lower COF and wear rate values compared with a pure DLC film in humid air.

In contrast, the COF of the Cr-H-DLC film is higher than the pure DLC film, which should reflect an increase in internal stresses owing to the incorporation of hydrogen into the film (Ref 30, 35). Generally, atomic hydrogen can saturate the C=C bonds, mainly converting  $sp^2$ -C to  $sp^3$ -CH, which leads to an increase in the  $sp^3$  fraction within the DLC film (Ref 35, 47). This is also consistent with the results shown in Fig. 3 and Table 4. Therefore, the Cr-H-DLC film presents a higher COF and poorer wear resistance than the Cr-DLC film in humid air.

Another mechanism that could affect the friction and wear behaviors of DLC films is the sliding environment. Although the tests were performed in air at room temperature with relative humidity of  $27 \pm 2\%$ , the sliding environment was found to have little effect on the friction and wear behaviors of the films, and therefore, it was neglected in further discussion.

**3.4.2 In DI Water.** To investigate the friction and wear behaviors of the bare and coated Mg alloy samples in water, the tests were performed in DI water. During the tests, it was found that the samples were prone to premature bearing failure under heavy loads such as 5 N. Therefore, a load of 1 N was used, as shown in Fig. 9-12. Compared with Fig. 7, the samples display different friction behaviors in Fig. 9. Initially, the COF of the bare Mg alloy is stable, but it fluctuates dramatically within the range of 0.31-0.39 after 500 s of sliding time. The COF of the Cr-DLC-coated Mg alloy fluctuates within the range of 0.11-0.19. The COF values of the pure DLC and Cr-H-DLC films have small fluctuations within the ranges of 0.08-0.10 and 0.07-0.13, respectively. Although the COF of the pure DLC film is more stable than the Cr-H-DLC film, the COF of the Cr-H-DLC film decreases gradually with increasing sliding time, i.e., it becomes much lower than the pure DLC film by the final step. This indicates that the Cr-H-DLC film would show better friction behavior in water in comparison with the pure DLC film.

Figure 10 shows the microscopy images of the wear scars of the bare and coated Mg alloys under loads of 1 N in DI water.

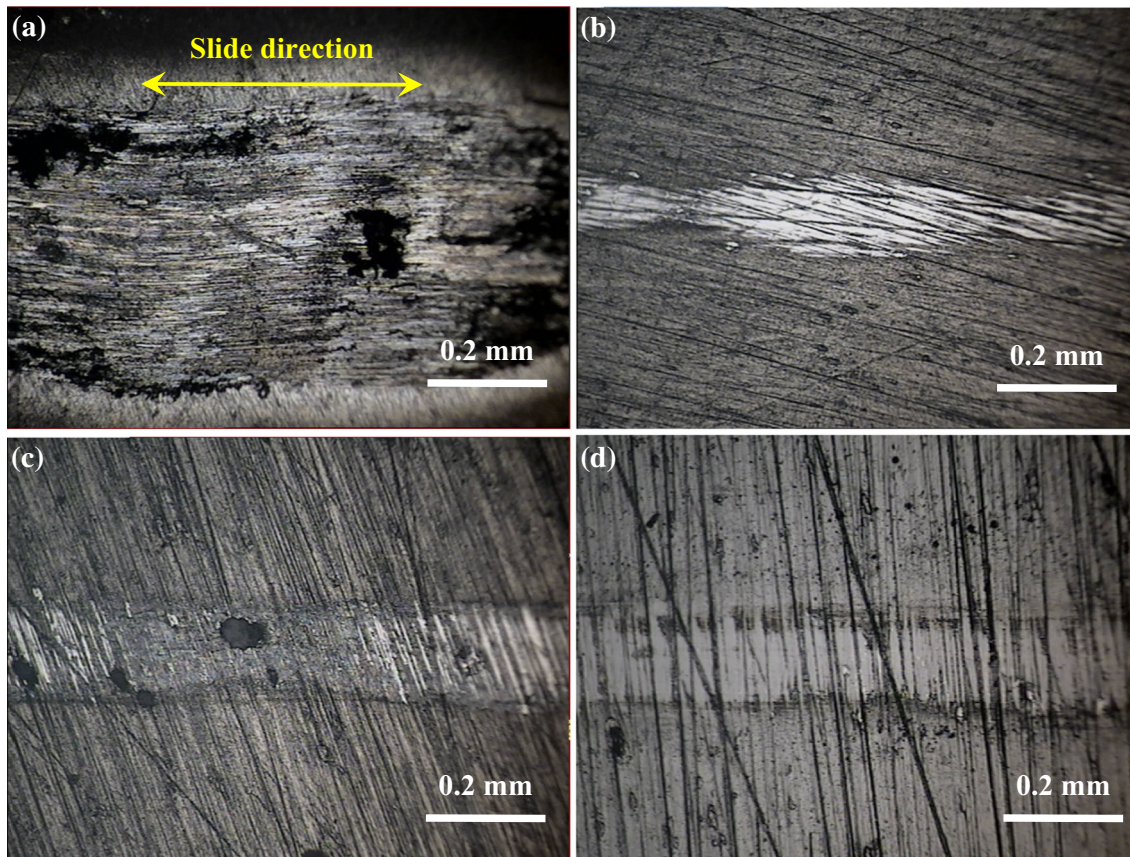


**Fig. 10** Microscope images of the wear scar of the bare and coated AZ91D Mg alloys at 1 N load in DI water. (a) Bare AZ91D; (b) DLC; (c) Cr-DLC; (d) Cr-H-DLC

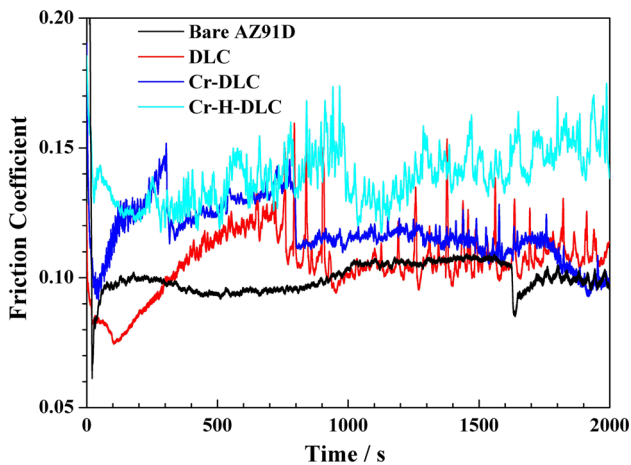


**Fig. 11** COFs of the bare and coated AZ91D Mg alloys as a function of the sliding time at 1 N load in 3.5 wt.% NaCl solution

The bare Mg alloy shows a wider wear track compared with that of the coated samples; it also has the highest wear rate in Table 4. Corrosion pits can be observed on the wear track of the Cr-DLC-coated Mg alloy (Fig. 10c), whereas pitting is not evident for the pure DLC and Cr-H-DLC samples. These corrosion pits could be responsible for the fluctuation of the COF of the Cr-DLC film. It can be concluded that the Cr-DLC film shows poor wear resistance in DI water. In addition,

according to Table 4, the order of wear rate from large to small is bare Mg alloy > Cr-DLC > pure DLC > Cr-H-DLC. Therefore, of the samples tested, the Cr-H-DLC film provides the best wear protection for Mg alloy in DI water.

If lubricant water was added onto the friction surface, the wear debris (Mg and MgO) from the bare Mg alloy would react with the water molecules to form insoluble  $Mg(OH)_2$  as the main corrosion product (Ref 41). Insoluble  $Mg(OH)_2$ , as new abrasive particles, could increase the frictional resistance, resulting in an increase and greater fluctuation of the COF. Additionally, water molecules could penetrate via the micro-/nanopores into the DLC films, forming micro-/nanogalvanic cells between the DLC/Cr layer and the substrate (Ref 10, 28). Therefore, synergistic effects between galvanic corrosion and chemical wear could accelerate the failure of DLC films during the tests. The above shows that the corrosion protection offered by the Cr-DLC film is less than that of the pure DLC- and Cr-H-DLC-coated samples; thus, this explains the severe corrosion observed on the Cr-DLC-coated Mg alloy. Therefore, the compactness of a DLC film plays an important role in the corrosion resistance offered to the coated Mg alloys in DI water.

**3.4.3 In NaCl Solution.** Figure 11 shows the COF values of bare and coated Mg alloys as a function of sliding time under a load of 1 N in 3.5 wt.% NaCl solution. The COF values of the coated Mg alloys fluctuate widely, while those of the bare Mg alloy remains comparatively stable. The stable COF of the bare Mg alloy varies in the range of 0.09-0.11, whereas the COF



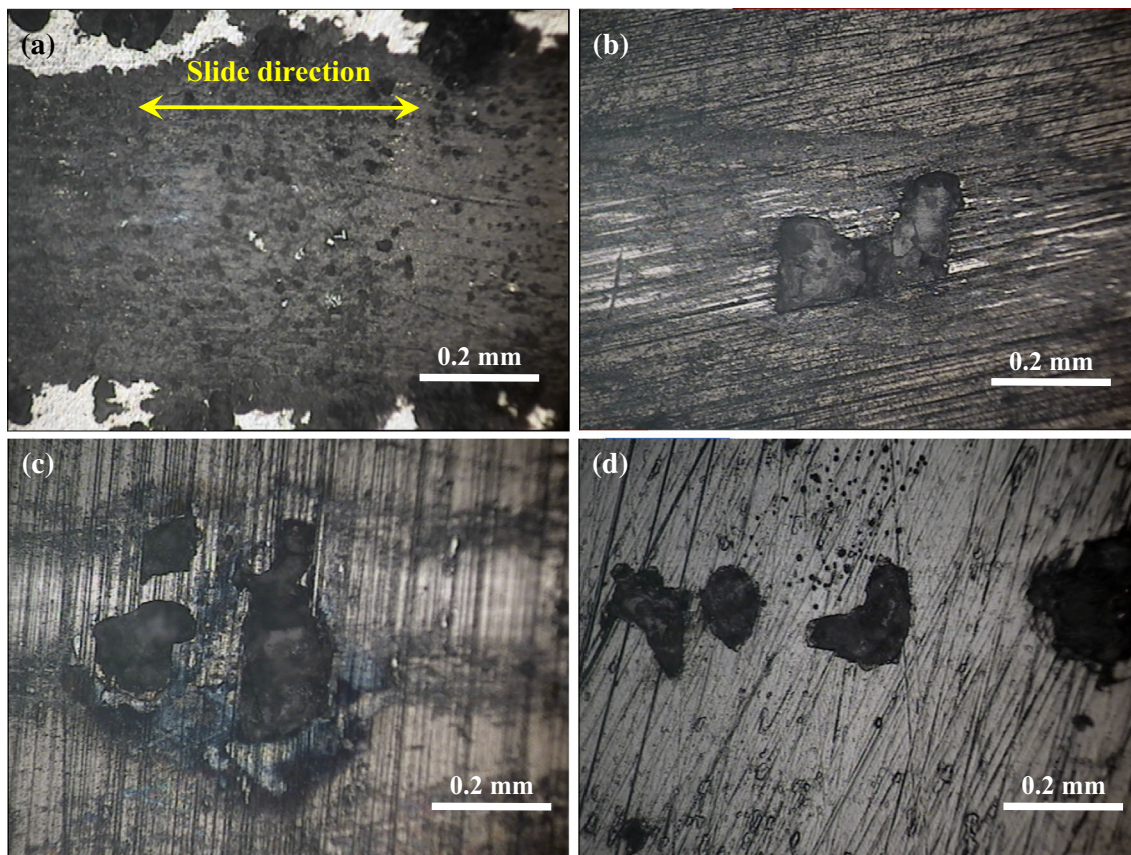


**Fig. 12** Microscope images of the wear scar of the bare and coated AZ91D Mg alloys at 1 N load in 3.5 wt.% NaCl solution. (a) Bare AZ91D; (b) DLC; (c) Cr-DLC; (d) Cr-H-DLC

values for all the coated samples are higher with broader ranges of fluctuation. Moreover, the COF values of the coated samples exhibit the same trends of change, i.e., they increase to a maximum value and then decrease suddenly; it is just the sliding times that are different.

Figure 12 exhibits microscope images of wear scars of the bare and coated Mg alloys under loads of 1 N in 3.5 wt.% NaCl solution. The bare Mg alloy shows a wider wear track compared with the coated samples. In contrast, the wear scars of the coated samples appear to incorporate several large corrosion pits, whereas the wear scar of the bare substrate shows only small corrosion pits, characteristic of typical corrosion wear.

Compared with the friction and wear behaviors of the bare substrate in DI water (Fig. 9 and 10a), the worn bare substrate in the NaCl solution shows a low COF, high rate of wear (Table 4), and an absence of grooves or plows on the wear scar. This reveals that the bare Mg alloy presents good friction behavior (low COF) but poor wear resistance in a Cl-containing solution. Comparably, the Cr-DLC-coated sample shows much greater corrosion than the other coated samples, evidenced by the bigger corrosion pits. This could be ascribed to the poor anticorrosion properties of the Cr-DLC-coated sample. Nevertheless, the coated Mg alloys showed very limited endurance, and they could not survive the NaCl solution. Thus, it can be concluded that compactness of DLC films is vital in affording protection to Mg alloys.

### 3.5 Discussion

**3.5.1 Improvement of Corrosion Protection Capability of DLC Films.** It is apparent from Fig. 1 and 2 that the Cr-H-DLC film shows better compactness than the pure DLC and Cr-DLC films, resulting in higher corrosion resistance of the Cr-H-DLC-coated Mg alloy compared with the other studied samples. Thus, it is evident that DLC films with higher compactness afford better corrosion protection.

Defects such as cracks, pinholes, or pores are difficult to avoid in DLC films when they are fabricated using PVD techniques (Ref 36-38), i.e., galvanic corrosion or a corrosion microcell might occur in such defects when the coated samples are within corrosive environments. In this study, Cr was found responsible for the poor corrosion resistance of the Mg alloy coated in the pure DLC film because of the high potential difference between Cr ( $-0.913$  versus SHE) and Mg ( $-2.363$  versus SHE). Furthermore, Wu et al. (Ref 12, 48) reported that the corrosion of Mg alloys could be accelerated if Al, Ti, or Cr was used as an interlayer between the Mg alloy and the hard coating because of the formation of galvanic cells; however, of the three, an interlayer of Al is preferred for impeding the corrosion of the Mg alloy. Therefore, another feasible method to inhibit corrosion should be to decrease the galvanic potential difference between the Mg alloy and the coating when a galvanic cell is produced.

Electrical conductivity should also be considered to enhance the corrosion protection capability of DLC films. This study

showed that the corrosion resistance of the Cr-DLC-coated Mg alloy was less than that of the pure DLC-coated sample, which could be attributed to an increase in the electrical conductivity due to Cr doping. Conversely, Masami et al. (Ref 49) proved that the corrosion protection of Si-DLC/Ti is better than Ti-DLC/Ti on AZ91 Mg alloy. Therefore, to improve the corrosion resistance of Mg alloys using DLC films, the following suggestions should be considered:

- (1) Improve the compactness of the DLC film.
- (2) Decrease the potential difference between the substrate and the buffer layer or film.
- (3) Reduce the electrical conductivity of the film or use inert metal doping.

**3.5.2 Key to Enhancing the Friction and Wear of DLC Films.** According to normal friction and wear theory, softer materials should experience greater wear than harder materials when two dissimilar materials rub against each other (Ref 8, 25). Thus, compared with the bare Mg alloy, all the DLC-coated samples considered in this study presented good friction and wear behaviors regardless of the test environment. Furthermore, comparably, the COF of the Cr-H-DLC film was found higher than that of the pure DLC and Cr-DLC films in air, resulting in a higher wear rate; however, the Cr-DLC-coated sample showed the lowest COF and wear rate values. Therefore, a metal-doped DLC film (e.g., Cr-DLC) has better friction and wear properties that offer greater wear protection for Mg alloys in air.

In addition, the interface bonding strength has a vital influence on the wear resistance of the DLC films (Ref 13, 15). The differences between the DLC film and Mg alloy in material properties, such as the hardness, elastic modulus, and melting points, as well as the high internal stress of the DLC film, would dramatically reduce the adhesive strength of the DLC film on the Mg alloy. The increasing adhesion strength between the Cr-DLC film and AZ91D Mg alloy (Fig. 4) is attributed to the transition layer of Cr in the interface, as it leads to good dry friction and wear properties in air (Fig. 7 and 8). Therefore, a transition layer between the hard DLC film and soft Mg alloy must exist to obtain the high adhesion.

Under environmental conditions of water or NaCl solution, in addition to their inherent characteristics, friction, and wear behaviors of the DLC films must reflect their capability to protect Mg alloys against corrosion. In water, the COF values of the pure DLC and Cr-H-DLC films were found low and stable, whereas that of the Cr-DLC film was high and fluctuating (Fig. 9). Moreover, corrosion pits were observed on the Cr-DLC-coated sample but not on the pure DLC- and Cr-H-DLC-coated samples (Fig. 10). When subjected to corrosive media such as NaCl solution, the properties of the Cr-DLC film deteriorated (Fig. 12). Although the pure DLC and Cr-H-DLC films showed reasonable protection against corrosion for the Mg alloy in NaCl solution (Fig. 5 and 6), they demonstrated only limited protection with severe corrosion evident on the Mg alloy during the wear tests in a corrosive solution. Therefore, the capability of DLC films for protecting Mg alloy against corrosion has a vital role in their friction and wear behaviors in water or NaCl solution.

## 4. Conclusions

- (1) The Cr-H-DLC film exhibited better compactness than the pure DLC and Cr-DLC films, resulting in a reasonable capability to protect the Mg alloy against corrosion. However, the Cr-DLC film accelerated the corrosion of the Mg alloy, which could be attributed to increased electrical conductivity resulting from Cr doping and the high potential difference between Cr and Mg.
- (2) Compared with the bare Mg alloy, all DLC-coated samples showed lower values of COF and smaller rates of wear, regardless of the environment (i.e., humid air, deionized water, or 3.5 wt.% NaCl solution). Of all the tested samples, the Cr-DLC-coated Mg alloy displayed the best friction and wear properties for the protection of Mg alloys in air but the poorest properties in water and NaCl solution.
- (3) The corrosion protection ability of DLC films plays a vital role in their wear resistance protection for Mg alloys in water or NaCl solution. Thus, to enhance the corrosion protection capability of DLC films, an ideal DLC film should exhibit characteristics of perfect compactness, high adhesive strength, low galvanic potential between the substrate and the buffer layer or film, and high electrical resistance.

## Acknowledgment

This work was supported by the Science and Technology Planning Project of Sichuan Province (2016JZ0032), the Key Laboratory of Marine Materials and Related Technologies, Ningbo Institute of Materials Technology and Engineering, Chinese Academy of Sciences (2018Z01), and the National Natural Science Foundation of China (51865017). The authors thank Lin-Chuan Gu and Yong-Sheng Jiang for their assistance in the experiments.

## References

1. S.H. You, Y.D. Huang, K.U. Kainer, and N. Hort, Recent Research and Developments on Wrought Magnesium Alloys, *J. Magn. Alloys*, 2017, **5**, p 239–253
2. X.J. Wang, D.K. Xu, R.Z. Wu, X.B. Chen, Q.M. Peng, L. Jin, Y.C. Xing, Z.Q. Zhang, Y. Liu, X.H. Chen, G. Chen, K.K. Deng, and H.Y. Wang, What is Going on in Magnesium Alloys, *J. Mater. Sci. Technol.*, 2018, **34**, p 245–247
3. G.L. Song, Recent Progress in Corrosion and Protection of Magnesium Alloys, *Adv. Eng. Mater.*, 2005, **7**, p 563–586
4. F.Y. Cao, G.L. Song, and A. Atrens, Corrosion and Passivation of Magnesium Alloys, *Corros. Sci.*, 2016, **111**, p 835–845
5. X.J. Cui and J. Ping, Research Progress of Microarc Oxidation for Corrosion Protection of Mg-Alloys, *J. Chin. Soc. Corr. Prot.*, 2018, **38**, p 87–104 (in Chinese)
6. R.M. Asmussen, W.J. Binns, P. Jakupi, and D. Shoesmith, Microstructural Effects on Corrosion of AM50 Magnesium Alloys, *J. Electrochem. Soc.*, 2014, **161**(10), p C501–C508
7. J. Choi, S. Nakao, J. Kim, M. Ikeyama, and T. Katob, Corrosion Protection of DLC Coatings on Magnesium Alloy, *Diam. Relat. Mater.*, 2007, **16**, p 1361–1364
8. N. Yamauchi, K. Demizu, N. Ueda, N.K. Cuong, T. Sone, and Y. Hirose, Friction and Wear of DLC Films on Magnesium Alloy, *Surf. Coat. Technol.*, 2005, **193**, p 277–282



9. J. Choi, J. Kim, S. Nakao, M. Ikeyama, and T. Kato, Friction Properties of Protective DLC Films on Magnesium Alloy in Aqueous NaCl Solution, *Nucl. Instrum. Methods B*, 2007, **257**, p 718–721
10. G.S. Wu, W. Dai, H. Zheng, and A.Y. Wang, Improving Wear Resistance and Corrosion Resistance of AZ31 Magnesium Alloy by DLC/AlN/Al Coating, *Surf. Coat. Technol.*, 2010, **205**, p 2067–2073
11. Y. Sun, C. Lu, H.L. Yu, A. KietTieu, L.H. Su, Y. Zhao, H.T. Zhu, and C. Kong, Nanomechanical Properties of TiCN and TiCN/Ti Coatings on Ti Prepared by Filtered Arc Deposition, *Mater. Sci. Eng. A*, 2015, **625**, p 56–64
12. G.S. Wu, L.L. Sun, W. Dai, L.X. Song, and A.Y. Wang, Influence of Interlayers on Corrosion Resistance of Diamond-Like Carbon Coating on Magnesium Alloy, *Surf. Coat. Technol.*, 2010, **204**, p 2193–2196
13. A.Y. Wang, K.R. Lee, J.P. Ahn, and J.H. Han, Structure and Mechanical Properties of W Incorporated Diamond-Like Carbon Films Prepared by a Hybrid Ion Beam Deposition Technique, *Carbon*, 2006, **44**, p 1826–1832
14. W. Yang, P.L. Ke, Y. Fang, H. Zheng, and A.Y. Wang, Microstructure and Properties of Duplex (Ti:N)-DLC/MAO Coating on Magnesium Alloy, *Appl. Surf. Sci.*, 2013, **270**, p 519–525
15. W. Dai, G.S. Wu, and A.Y. Wang, Preparation, Characterization and Properties of Cr Incorporated DLC Films on Magnesium Alloy, *Diam. Relat. Mater.*, 2010, **19**, p 1307–1315
16. W. Dai and A.Y. Wang, Deposition and Properties of Al-Containing Diamond-Like Carbon Films by a Hybrid Ion Beam Sources, *J. Alloys Compd.*, 2011, **509**, p 4626–4631
17. G.A. Zhang, P.X. Yan, P. Wang, Y.M. Chen, J.Y. Zhang, L.P. Wang, and J.Y. Zhang, The Effect of Applied Substrate Negative Bias Voltage on the Structure and Properties of Al-Containing aC: H Thin Films, *Surf. Coat. Technol.*, 2008, **202**, p 2684–2689
18. X. Fan, E.C. Dickey, S.J. Pennycook, and M.K. Sunkara, Z-Contrast Imaging and Electron Energy-Loss Spectroscopy Analysis of Chromium-Doped Diamond-Like Carbon Films, *Appl. Phys. Lett.*, 1999, **75**, p 2740–2742
19. Y.M. Wu, S.G. Zhou, W.J. Zhao, and L. Ouyang, Comparative Corrosion Resistance Properties Between (Cu, Ce)-DLC and Ti Co-Doped (Cu, Ce)/Ti-DLC Films Prepared Via Magnetron Sputtering Method, *Chem. Phys. Lett.*, 2018, **8**, p 50–58
20. V. Singh, J.C. Jiang, and E.I. Meletis, Cr-Diamond Like Carbon Nanocomposite Films: Synthesis, Characterization and Properties, *Thin Solid Films*, 2005, **489**, p 150–158
21. S. Viswanathan, L. Mohan, P. Bera, V.P. Kumar, H.C. Barshilia, and C. Anandan, Corrosion and Wear Behaviors of Cr-Doped Diamond-Like Carbon Coatings, *J. Mater. Eng. Perform.*, 2017, **26**, p 3633–3647
22. A. Amanov, T. Watabe, R. Tsuboi, and S. Sasaki, Fretting Wear and Fracture Behaviors of Cr-Doped and Non-doped DLC Films Deposited on Ti-6Al-4V Alloy by Unbalanced Magnetron Sputtering, *Tribol. Int.*, 2013, **62**, p 49–57
23. C.W. Zou, H.J. Wang, L. Feng, and S.W. Xue, Effects of Cr Concentrations on the Microstructure, Hardness, and Temperature-Dependent Tribological Properties of Cr-DLC Coatings, *Appl. Surf. Sci.*, 2013, **286**, p 137–141
24. W. Dai and A.Y. Wang, Synthesis, Characterization and Properties of the DLC Films with Low Cr Concentration Doping by a Hybrid Linear Ion Beam System, *Surf. Coat. Technol.*, 2011, **205**, p 2882–2886
25. Q.Z. Wang, F. Zhou, X.D. Ding, Z.F. Zhou, C.D. Wang, W.J. Zhang, L.K.-Y. Li, and S.T. Lee, Structure and Water-Lubricated Tribological Properties of Cr/a-C Coatings with Different Cr Contents, *Tribol. Int.*, 2013, **67**, p 104–115
26. X.D. Sui, J.Y. Liu, S.T. Zhang, J. Yang, and J.Y. Hao, Microstructure, Mechanical and Tribological Characterization of CrN/DLC/Cr-DLC Multilayer Coating with Improved Adhesive Wear Resistance, *Appl. Surf. Sci.*, 2018, **439**, p 24–32
27. Q.Z. Wang, F. Zhou, Z.F. Zhou, C.D. Wang, W.J. Zhang, L.K.-Y. Li, and S.T. Lee, Effect of Titanium or Chromium Content on the Electrochemical Properties of Amorphous Carbon Coatings in Simulated Body Fluid, *Electrochim. Acta.*, 2013, **112**, p 603–611
28. A. Zeng, E. Liu, I.F. Annergren, S.N. Tan, S. Zhang, P. Hing, and J. Gao, EIS Capacitance Diagnosis of Nanoporosity Effect on the Corrosion Protection of DLC Films, *Diam. Relat. Mater.*, 2002, **11**, p 160–168
29. N. Fujisawa, D.R. McKenzie, N.L. James, J.C. Woodard, and M.V. Swain, Combined Influences of Mechanical Properties and Surface Roughness on the Tribological Properties of Amorphous Carbon Coatings, *Wear*, 2006, **260**, p 62–74
30. M. Weiler, S. Sattel, T. Giessen, K. Jung, H. Ehrhardt, V.S. Veerasamy, and J. Robertson, Preparation and Properties of Highly Tetrahedral Hydrogenated Amorphous Carbon, *Phys. Rev. B*, 1996, **53**, p 1594–1608
31. Y. Taki and O. Takai, XPS Structural Characterization of Hydrogenated Amorphous Carbon Thin Films Prepared by Shielded Arc Ion Plating, *Thin Solid Films*, 1998, **316**, p 45–50
32. J.X. Liao, W.M. Liu, T. Xu, and Q.J. Xue, Characteristics of Carbon Films Prepared by Plasma-Based Ion Implantation, *Carbon*, 2004, **42**, p 387–393
33. J. Robertson, Diamond-Like Amorphous Carbon, *Mater. Sci. Eng. R*, 2002, **32**, p 129–281
34. D. Beeman, J. Silverman, R. Lynds, and M.R. Anderson, Modeling Studies of Amorphous Carbon, *Phys. Rev. B*, 1984, **30**, p 870–875
35. T. Mikami, H. Nakazawa, M. Kudo, and M. Mashita, Effects of Hydrogen on Film Properties of Diamond-Like Carbon Films Prepared by Reactive Radio-Frequency Magnetron Sputtering Using Hydrogen Gas, *Thin Solid Films*, 2005, **488**, p 87–92
36. P. Panjan, M. Cekada, M. Panjan, D. Kek-Merl, F. Zupani, L. Curkovi, and S. Paskvale, Surface Density of Growth Defects in Different PVD Hard Coatings Prepared by Sputtering, *Vacuum*, 2012, **86**, p 794–798
37. P. Panjan, M. Cekada, M. Panjan, and D. Kek-Merl, Growth Defects in PVD Hard Coatings, *Vacuum*, 2010, **84**, p 209–214
38. M. Fenker, M. Balzer, and H. Kappl, Corrosion Protection with Hard Coatings on Steel: Past Approaches and Current Research Efforts, *Surf. Coat. Technol.*, 2014, **257**, p 182–205
39. A.A. Voevodin, J.P. O'Neill, and J.S. Zabinski, Nanocomposite Tribological Coatings for Aerospace Applications, *Surf. Coat. Technol.*, 1999, **116–119**, p 36–45
40. S.R. Polaki, N. Kumar, K. Ganesan, K. Madapu, A. Bahuguna, M. Kamruddin, S. Dash, and A.K. Tyagi, Tribological Behavior of Hydrogenated DLC Film: Chemical and Physical Transformations at Nano-Scale, *Wear*, 2015, **338**, p 105–113
41. S. Feliu, Jr., C. Maffiotte, A. Samaniego, J.C. Galván, and V. Barranco, Effect of Naturally Formed Oxide Films and Other Variables in the Early Stages of Mg-Alloy Corrosion in NaCl Solution, *Electrochim. Acta*, 2011, **56**, p 4554–4565
42. L. Wang, T. Shinohara, and B.P. Zhang, Influence of Chloride, Sulfate and Bicarbonate Anions on the Corrosion Behavior of AZ31 Magnesium Alloy, *J. Alloys Compd.*, 2010, **496**, p 500–507
43. S. Feliu, Jr., C. Maffiotte, J.C. Galvan, and V. Barranco, Atmospheric Corrosion of Magnesium Alloys AZ31 and AZ61 Under Continuous Condensation Conditions, *Corros. Sci.*, 2011, **53**, p 1865–1872
44. W. Dai, P.L. Ke, and A.Y. Wang, Microstructure and Property Evolution of Cr-DLC Films with Different Cr Content Deposited by a Hybrid Beam Technique, *Vacuum*, 2011, **85**, p 792–797
45. J. Andersson, R.A. Erck, and A. Erdemir, Friction of Diamond-Like Carbon Films in Different Atmospheres, *Wear*, 2003, **254**, p 1070–1075
46. A. Erdemir, The Role of Hydrogen in Tribological Properties of Diamond-Like Carbon Films, *Surf. Coat. Technol.*, 2001, **146–147**, p 292–297
47. A.P. Dementjev and M.N. Petukhov, The Roles of H and O Atoms in Diamond Growth, *Diam. Relat. Mater.*, 1997, **6**, p 486–489
48. G.S. Wu, A. Shanaghi, Y. Zhao, X.M. Zhang, R.Z. Xu, Z.W. Wu, G.Y. Li, and P.K. Chu, The Effect of Interlayer on Corrosion Resistance of Ceramic Coating/Mg Alloy Substrate in Simulated Physiological Environment, *Surf. Coat. Technol.*, 2012, **206**, p 4892–4898
49. I. Masami, N. Setsuo, S. Tsutomu, and C. Junho, Improvement of Corrosion Protection Property of Mg-Alloy by DLC and Si-DLC Coatings with PBII, Technique and Multi-target DC-RF Magnetron Sputtering, *Nucl. Instrum. Methods B*, 2009, **267**, p 1675–1679